A Modified BPaL Regimen for Tuberculosis Treatment replaces Linezolid with Inhaled Spectinamides

Malik Zohaib Ali [1,2,6], Taru S. Dutt [1,2], Amy MacNeill [2], Amanda Walz [1,2], Johnathan Patterson[1,2], Camron Pearce [1,2.6], Ha Lam[1,2], Marcela Henao-Tamayo[2], Richard E. Lee [3], Jiuyu Liu [3], Gregory T. Robertson [1,2], Anthony J. Hickey [4], Bernd Meibohm [5], Mercedes Gonzalez-Juarrero [1,2]

[1]Mycobacteria Research Laboratories, Colorado State University, 80523, USA

[2] Microbiology, Immunology and Pathology, Colorado State University, 80523, USA

[3] Department of Chemical Biology and Therapeutics, St. Jude Children's Research Hospital, 38105, USA

[4]Technology Advancement and Commercialization, RTI International, 27709, USA

[5] Department of Pharmaceutical Sciences, University of Tennessee Health Science Center, 38163, USA

[6] Program in Cell & Molecular Biology, Colorado State University, 80523, USA

Keywords: mycobacterium tuberculosis, inhalation, spectinamides , BPaL, linezolid, MDR-TB, XDR-TB, therapy, multidrug regimen , C3HeB/FeJ mice , Balb/c mice , 1599

Corresponding Author Information: Mercedes.gonzalez-juarrero@colostate.edu

Abstract

The Nix-TB clinical trial evaluated a new 6-month regimen containing three-oral-drugs; bedaquiline (B), pretomanid (Pa) and linezolid (L) (BPaL regimen) for treatment of tuberculosis (TB). This regimen achieved remarkable results as almost 90% of the multidrug resistant (MDR) or extensively drug resistant (XDR) TB participants were cured but many patients also developed severe adverse effects (AEs). The AEs were associated with the long-term administration of the protein synthesis inhibitor linezolid. Spectinamide 1599 (S) is also a protein synthesis inhibitor of *Mycobacterium tuberculosis* with an excellent safety profile but which lacks oral bioavailability. Here we hypothesize that inhaled spectinamide 1599, combined with BPa —BPaS regimen—has similar efficacy to that of BPaL regimen while simultaneously avoiding the L-associated AEs. The BPaL and BPaS regimens were compared in the Balb/c and C3HeB/FeJ murine chronic TB efficacy models. After 4-weeks of treatment, both regimens promoted equivalent bactericidal effect in both TB murine models. However, treatment with BPaL resulted in significant weight loss and the complete blood count suggested development of anemia. These effects were not similarly observed in mice treated with BPaS. BPaL treatment also decreased myeloid to erythroid ratio and increased concentration of proinflammatory cytokines in bone marrow compared to mice receiving BPaS regimen. During therapy both regimens improved the lung lesion burden, reduced neutrophil and cytotoxic T cells counts while increased the number of B and helper and regulatory T cells. These combined data suggest that inhaled spectinamide 1599 combined with BPa is an effective TB regimen that avoids L-associated AEs.

IMPORTANCE Tuberculosis (TB) is an airborne infectious disease that spreads via aerosols containing *Mycobacterium tuberculosis* (Mtb), the causative agent of TB. TB can be cured by administration of 3-4 drugs for 6-9 months but there are limited treatment options for patients infected with multidrug (MDR) and extensively resistant (XDR) strains of Mtb. BPaL is a new all-oral combination of drugs consisting of Bedaquiline (B), Pretomanid (Pa) and Linezolid (L). This regimen was able to cure ~90% of MDR and XDR TB patients in clinical trials but many patients developed severe adverse effects (AEs) associated to the long-term administration of linezolid. We evaluated a new regimen in which Linezolid in the BPaL regimen was replaced with inhaled spectinamide 1599. In the current study, we demonstrate that 4-weeks of treatment with inhaled spectinamide 1599 in combination with Bedaquiline and Pretomanid has equivalent efficacy to the BPaL drug combination and avoids the L-associated-AEs.

63 **Introduction**

64 Tuberculosis (TB) remains one of the leading causes of death initiated by an
65 infectious agent. In 2021, the World Health Organization reported 10.6 million new TB
66 cases worldwide and among those, 450,000 cases were also diagnosed as multidrug
67 resistant (MDR) or extensively drug resistant (XDR) TB (1). Treatment of MDR- and XDR-
68 TB patients is lengthy and is often poorly tolerated due to significant associated side
69 effects (2).

70 Recently, a 6-month novel treatment regimen of three-oral-drugs: bedaquiline (B),
71 pretomanid (Pa) and linezolid (L) referred to as the BPaL regimen was approved.
72 Preclinical studies demonstrated the better efficacy of BPaL regimen for drug sensitive
73 TB compared to the standard TB chemotherapy (1,3,4) and thereafter, the BPaL regimen
74 was tested in the Nix-TB clinical trial conducted in South Africa (5). This trial enrolled
75 patients with XDR-TB and treatment-intolerant or non-responsive MDR-TB, including HIV
76 positive patients with a CD4 count of 50 or higher. The results were remarkable as 95 out
77 of 107 patients were cured though many patients had a high rate of treatment-associated
78 adverse effects (AEs).

79 The long-term administration of linezolid (an oxazolidinone antibiotic) was likely
80 the causative agent resulting in bone marrow myelosuppression (48%), peripheral
81 neuropathy, optic neuritis (81%) and anemia (37%) in patients treated with the BPaL
82 regimen (5). Subsequently, the ZeNix trial adjusted the BPaL regimen to a linezolid dose
83 of 600mg. This trial also had remarkable results; it cured 84-91% of patients (9 to 26
84 weeks of therapy, respectively) and resulted in fewer AEs than those observed in the Nix-
85 TB trial (6). Apart from AEs, several studies have also raised awareness of high doses of

86 linezolid leading to development of linezolid-resistant *Mycobacterium tuberculosis* (Mtb)
87 (7–9). At present, the TB-drug development field is working to modify the BPaL regimen
88 to maintain or improve its efficacy while diminishing treatment-associated AEs (10).

89 Spectinomycin, an aminocyclitol antibiotic, is a broad spectrum antibiotic used
90 mainly for the treatment of *Neisseria gonorrhoeae* (11). It inhibits bacterial protein
91 synthesis (12) and has a very high safety profile with no known ototoxicity and
92 nephrotoxicity (13,14). The efficacy of spectinomycin against Mtb is very poor but its
93 structural modification led to the development of a new series of semisynthetic analogs
94 called spectinamides (12,15,16). Spectinamides bind selectively with the bacterial 30S
95 ribosomes and importantly, unlike linezolid, they do not bind to the mitochondrial 30S in
96 mammalians cells. The latter represents a great advantage for reduced potential for side
97 effects, such as ototoxicity and myeloid suppression that are commonly associated with
98 other protein synthesis inhibitors such as amikacin and linezolid, respectively (17,18).
99 Spectinamides' potent anti-tubercular activity is attributed to its ability to evade drug efflux
100 by Rv1258c major facilitator superfamily transporter present on the surface of Mtb
101 (19,20). Spectinamides have shown excellent activity against MDR- and XDR-Mtb strains
102 (16,21). However, their poor oral availability have limited their usage to injectable forms.

103 One of the lead spectinamides, 1599, has demonstrated promising results *in vitro*
104 and *in vivo* and was shown to lack cross-resistance with existing anti-TB drugs (16,19–
105 23). 1599, delivered subcutaneously, proved an effective partner agent when combined
106 with rifampin and pyrazinamide and also with bedaquiline, pretomanid or moxifloxacin in
107 TB mouse efficacy models of increasing complexity (21).

108 One of the limitations of using 1599 as injectable is a potential risk for poor patient
109 compliance (24) and direct administration of aerosolized antibiotics to the lungs has been
110 studied for decades as an alternative to systemic drug administration via injection.
111 Aerosolized administration of 1599 has been tested in preclinical *in vivo* studies using
112 liquid formulation of the drug. These studies have shown that inhaled 1599, used in
113 monotherapy or in combination with pyrazinamide, is efficacious and well tolerated in
114 murine TB efficacy models (25,26). A comparative study assessing biodistribution of the
115 drug in relation to the administration route demonstrated that 1599 showed 48 times
116 higher exposure in mouse lungs via inhalation compared to equivalent dosages
117 administered by subcutaneous injection; the latter may explain the increased efficacy of
118 this drug following intrapulmonary aerosol (22,26). Moreover, 1599 was shown to be
119 amenable to dry powder formulation and delivery, suggesting a pathway to a more
120 patient-friendly delivery system (27). Therefore, in this study, we hypothesized that
121 combining BPa with inhaled S will maintain equivalent efficacy to the BPaL regimen while
122 avoiding the accompanying toxicities that occurred with long-term BPaL administration to
123 human MDR/XDR-TB patients.
124

125 **Results**

126 ***Linezolid and spectinamide 1599 show similar efficacy in monotherapy***

127 To compare the efficacy of L or S in monotherapy, Mtb-infected C3HeB/FeJ (n=7)
128 and Balb/c (n=4-6) mice received L (administered 5/7 days per week orally at 100 mg/Kg)
129 or S (administered 3/7 days per week on alternate days via intrapulmonary aerosol
130 delivery at 100 mg/Kg and 50 mg/Kg, respectively) for 4 weeks. At the end of treatment,

131 the animals were sacrificed, and the CFU in lungs and spleen was enumerated (Figure
132 1A-D). Treatment of C3HeB/FeJ mice with L (7.30 ± 0.45 $\log_{10}$) or S (6.90 ± 0.48 $\log_{10}$)
133 for 4 weeks resulted in an average of 0.51 and 0.91 $\log_{10}$ CFU reduction in the lungs
134 respectively, compared to untreated (UnRx) control (7.81 ± 0.36 $\log_{10}$) (Figure 1A). This
135 difference failed to achieve statistical significance owing to the larger standard deviation
136 associated with heterogenous advanced lung pathology observed in this model
137 (26,28,29). In contrast, L (4.49 ± 0.10 $\log_{10}$) treated C3HeB/FeJ mice had significantly
138 lower spleen bacterial burden compared to UnRx (5.43 ± 0.27 $\log_{10}$), with no significant
139 difference between the L and S (4.94 ± 0.11 $\log_{10}$) treatment arm (Figure 1C). In Balb/c
140 mice, L or S treatment was found to promote significant reduction in lung bacterial burden
141 (0.83 and 0.77 $\log_{10}$ respectively) compared to UnRx or the vehicle only controls (Figure
142 1B). There was no significant difference in lung bacterial burden after L or S treatment in
143 Balb/c mice and there was no change in spleen bacterial burden compared to UnRx
144 control (Figure 1D).
145
146 ***Combination therapy with BPaL or BPaS have similar efficacy***
147 We further tested and compared the efficacy of L or S when used in combination
148 therapy with BPa. Mtb-infected C3HeB/FeJ mice were treated with either BPaL (B=
149 25mpk; Pa= 100 mg/Kg and L= 100 mg/Kg all administered 5/7 a week via oral gavage)
150 or BPaS (BPa as in BPaL and S= 100 mg/Kg administered 3/7 a week on alternate days
151 via intrapulmonary aerosol delivery) for 4 weeks. The comparative analysis from
152 combined data of three independent studies is shown in Figure 1E&G (data from
153 individual studies are shown in Figures S1-3). Two of three studies contained an extra

154 group of BPa treated mice as a reference control. Compared to UnRx (7.48 ± 0.12 $\log_{10}$)
155 control, mice in the BPa (5.49 ± 0.42 $\log_{10}$), BPaL (4.76 ± 0.38 $\log_{10}$) and BPaS (4.98 ±
156 0.35 $\log_{10}$) treatment groups had significantly reduced the lung bacterial burden by 1.99,
157 2.72, and 2.50 $\log_{10}$ respectively (Figure 1E). Although a higher CFU reduction was
158 observed in the lungs of C3HeB/FeJ mice treated with BPaL or BPaS, these differences
159 failed to achieve statistical significance compared to BPa backbone regimen. All three
160 regimens proved highly effective at reducing spleen bacterial burden in C3HeB/FeJ mice,
161 with most mice returning no CFU within the limit of detection (LOD) employed herein
162 (Figure 1G).

163 The effect of BPaL and BPaS (S= 50 mg/Kg) combination therapy on the bacterial
164 burden in lungs and spleen of Mtb-infected Balb/c mice was determined at the end of 4-
165 weeks of treatment. Figure 1F&H show the combined lung and spleen CFU data from two
166 independent studies (data for each study is shown in Figures S7-8). The combined result
167 demonstrated that compared to UnRx (5.24 ± 0.17 $\log_{10}$) control, mice in the BPaL (1.29
168 ± 0.13 $\log_{10}$) and BPaS (1.44 ± 0.17 $\log_{10}$) treatment groups returned significantly fewer
169 CFU in the lungs, with most mice returning no CFU within the LOD employed herein
170 (Figure 1F). As in C3HeB/FeJ TB model, no significant difference was observed in the
171 lung CFU of Balb/c mice treated with either the BPaL or BPaS regimen. BPaL and BPaS
172 therapy reduced Balb/c spleen bacterial burden to below the LOD of the assay with no
173 CFU recovered for any treated mice (Figure 1H). In summary, these results support our
174 hypothesis and demonstrate that both BPaL and BPaS multidrug regimens show
175 equivalent bactericidal effects in C3HeB/FeJ and Balb/c chronic TB efficacy models.
176

177 **Monitoring of adverse effects**

178 Five approaches were employed to monitor treatment-associated AEs in mice in
179 this study including 1) changes in the live body weight of mice; 2) lung histopathology and
180 lesion scoring 3) evaluation of complete blood count (CBC), 4) clinical pathology to study
181 myelosuppression in bone marrow and 5) changes in content of immune cells in the lungs,
182 spleen, bone marrow and blood.

183

184 ***BPaL therapy decreases the live body weight of mice***

185 No significant difference in the live body weight among the treatment groups in
186 either C3HeB/FeJ or Balb/c mice was observed following 4-weeks of treatment with S or
187 L alone (Figure 2A&B). On the other hand, C3HeB/FeJ or Balb/c mice treated with BPa,
188 BPaL or BPaS showed marginal loses of live body weight, ranging from 2.37-5.13% and
189 only mice receiving the BPaL regimen, when compared to the UnRx control, reached
190 statistically significant loses in live body weight by the end of treatment (Figure 2C&D).

191

192 ***BPaL and BPaS therapy result in significant lower lung lesion burden***

193 The lesions in Mtb-infected UnRx C3HeB/FeJ mice (Figure 2E) showed a
194 spectrum of diverse granuloma types ranging from aggregations of macrophages and
195 lymphocytes to highly organized granulomas with collagen encapsulation and a region
196 of central caseous necrosis that resembles to those found in some human patients
197 (28,29). By comparison, lung lesions of Mtb-infected Balb/c mice (Figure 2G) consisted
198 of granulomas with a very homogeneous structure (28) formed also by aggregations of
199 macrophages and lymphocytes without a necrotic core. Mice treated for 4 weeks with

200 the BPaL or BPaS regimen presented with significant reduction in the number and size
201 of TB granulomas in both C3HeB/FeJ and Balb/c TB models compared to their
202 respective UnRx control, with no significant difference in lesion burden score between
203 the combination drug treatment groups (Figure 2F&H).
204
205 ***Association of L with altered blood profile and mild anemia in mice***
206 Complete blood count (CBC) profile was performed on Mtb-infected C3HeB/FeJ
207 mice at the end of 4-weeks of treatment to quantify treatment-associated hematological
208 changes. The results obtained from mice treated with L or S alone are summarized in
209 Figure 3A. Compared to UnRx control and S treated mice, L treatment significantly
210 increased the red blood cell distribution width standard deviation (RDWs), while both L
211 and S treatment were associated with a significant decrease in the mean corpuscular
212 hemoglobin concentration (MCHC) compared to UnRx control (Figure 3A).
213 The effect of combination therapy with the BPaL or BPaS regimen on CBC profile
214 was analyzed at 1-, 2- and 4-weeks of treatment (Figure 3B). None of the 20 parameters
215 of CBC changed during the first 2 weeks of treatment. However, L-containing BPaL
216 regimen was again associated with a significant increase in the RDWs, and lower
217 hemoglobin (HGB) compared to UnRx control after 4 weeks. This effect was not observed
218 in mice treated with BPa or BPaS (Figure 3B). However, as in monotherapy, there was a
219 trend towards lower overall MCHC in mice treated with either BPaL or BPaS. The mean
220 platelet volume (MPV) was marginally higher at 4 weeks in mice treated with BPa
221 compared to BPaL or BPaS, albeit not significantly different from UnRx control (Figure
222 3B). Given that no difference in HGB or RDWs was observed between UnRx control and

223 their comparator BPa and BPaS regimens, we concluded that the significant HGB
224 decrease and RDWs increase (often observed during development of anemia) were
225 associated with inclusion of L in BPaL regimen.
226
227 ***Spectinamide 1599 recovers the altered ratio of myeloid to erythroid cells in bone***
228 ***marrow***
229 To further evaluate if L was associated with myelosuppressive effect, we
230 performed hematopathology analysis on bone marrow from Mtb-infected C3HeB/FeJ and
231 Balb/c mice at the end of treatment. For C3HeB/FeJ mice, the number of myeloid (M) and
232 erythroid (E) precursor cells were calculated from H&E stained sections and their myeloid
233 to erythroid ratio (M:E) was determined by counting 300 bone marrow cells in 5 different
234 regions (Figure 3C). The BPa and BPaL treatment significantly decreased myeloid cells
235 while increasing the proportion of erythroid cells (Figure 3D). Hence, the corresponding
236 ratio in bone marrow of animals treated with BPaL or BPa was lower compared to UnRx
237 control. Importantly, the BPaS treatment did not show any difference in the content of
238 myeloid or erythroid cells when compared to UnRx control. In Mtb-infected Balb/c mice,
239 the number of myeloid and other cell types were counted, however, no significant
240 difference was found among the control and treatment groups (data not shown).
241
242 ***BPaL therapy increases proinflammatory cytokine response in bone marrow***
243 A comparative analysis for concentration of cytokines and chemokines in the bone
244 marrow, plasma, and lung samples from Mtb-infected C3HeB/FeJ mice treated with BPaL
245 or BPaS regimen was also conducted. The bone marrow samples demonstrated a

246 significant difference between the BPaL and BPaS groups, with appreciably higher level
247 of pro-inflammatory cytokines and chemokines (IL-1β, IL-12p70, IL-23, TNFα, GROα
248 (CXCL1), MP-2α (CXCL2), IP-10 (CXCL10), MP-1α (CCL3), RANTES (CCL5), MCP-3
249 (CCL7) and Eotaxin (CCL11)) in the BPaL- compared to BPaS-treated mice (Figure 4B).
250 The plasma and lung samples, however, had similar cytokine and chemokine contents
251 between the treatment groups except for MCP-3 (CCL7) in plasma which was significantly
252 higher in BPaS compared to BPaL group (Figure S11). We also performed a correlation
253 analysis of bone marrow cytokine and chemokine content with lung CFU obtained from
254 treatment (BPaL or BPaS) and UnRx groups (Figure 4C). The analysis suggested that
255 compared to UnRx control, there was a strong correlation between the pronounced
256 reduction of lung bacterial burden and profound reduction in bone marrow cytokine and
257 chemokine contents observed in mice from BPaL or BPaS groups. Similar correlations
258 were found between lung CFU and content of cytokines and chemokines in lung (Figure
259 S12) and plasma (Figure S13).
260
261 ***BPaL and BPaS therapies reduce inflammation-associated cells***
262 We further assessed the environment of immune cells using flow cytometry in
263 bone marrow, lungs, and blood from each group of Mtb-infected C3HeB/FeJ mice
264 (Figure 5). The bone marrow (Figure 5A) results revealed that as compared to UnRx
265 control, there was a significant decrease in the percentage of inflammatory myeloid
266 phenotypes (CD45+CD3-CD11b+CD11c-Ly6C+CCR2+, CD45+CD3-CD11b+CD11c-
267 Ly6C+CCR2+MHC-II+ and CD45+CD3-D14+CCR2+) in response to therapy with either
268 BPa, BPaL, or BPaS. In contrast, neutrophils (CD45+CD3-CD11b+CD11c-

269 Ly6C+Ly6G^{high}), precursor T cells (CD45+CD3+) and B cells (CD45+CD3-CD19+B220-)
270 were significantly increased in either BPa, BPaL, or BPaS treatment groups compared
271 to UnRx control in bone marrow. This reduced inflammatory response in treatment
272 groups is also consistent in blood shown by significantly reduced inflammatory myeloid
273 cells (CD45+CD3-CD11b+CD11c-Ly6C+CCR2+) (Figure 5B). Interestingly, the
274 response to therapy in the lungs (Figure 5C) was manifested by a significant increase of
275 CD3+CD4+ T helper cells and B-1 cells (CD3-CD19+) and a reverse trend for
276 CD3+CD8+ and γδ-T cells (CD3+CD8+γδTCR+).
277 Furthermore, we also assessed changes in the distribution of immune cells in the
278 lungs from Mtb-infected C3HeB/FeJ mice in response to therapy using multiplex
279 fluorescent immunohistochemistry (mfIHC). A 7-color composite image for cell markers
280 (B220, CD4, CD8, Foxp3, F4/80 and Ly6G) along with DAPI is shown in Figure 6A,
281 while their single-color staining is shown in Figure 6B. Figure 6A shows a typical
282 necrotic TB granuloma comprised of central necrosis, peripheral rim and lung
283 parenchyma. The analysis of mfIHC images revealed that the BPaL and BPaS
284 treatments significantly and dramatically lowered the number of neutrophils (count
285 based on Ly6G+) compared to UnRx control, however, F4/80+ cells were observed
286 significantly higher in BPaS compared to UnRx control (Figure 6C, S14). Interestingly,
287 the spearman's correlation plot (Figure 6D) shows that a significant decrease in
288 neutrophils was positively correlated with the corresponding increase in most of the
289 other immune cells.
290
291

292 **Discussion**

293 We used two preclinical chronic TB murine efficacy models (30–32) to investigate
294 BPa, BPaL and BPaS, for efficacy and any associated AEs during the course of 4-
295 weeks of treatment. Based on the diversity of outcomes observed during human TB
296 disease (22) and as no single animal model recapitulates the wide spectrum of human
297 TB pathology (33), we chose the Balb/c and C3HeB/FeJ murine TB models. The Balb/c
298 chronic TB model is representative of a long-term Mtb chronic infection that develops
299 homogenous lung granulomatous lesions restraining the bacilli within intracellular
300 compartments (34) of macrophages and foamy macrophages. In contrast, low-dose
301 aerosol Mtb infection of C3HeB/FeJ mice also results in a chronic infection, but their
302 lungs exhibit a heterogenous spectrum of lesions including granulomas similar to those
303 seen in Balb/c chronic TB model in addition to caseous necrotic lesions surrounded by a
304 fibrotic rim (28,29,35). The caseum of these necrotic granulomas creates a hypoxic
305 environment and contains abundant extracellular bacilli (28,29,36) in a similar fashion to
306 necrotic granulomas found in some human TB patients. It is believed that the fibrotic,
307 necrotic and hypoxic environment of these granulomas creates barriers to drug
308 penetration, alters bacterial phenotype, and all together challenge therapeutic outcomes
309 (30–32,37). Therefore, to understand the implications of drug efficacy and drug
310 associated AEs in scenario without (Balb/c) and with (C3HeB/FeJ) necrotic granulomas,
311 both murine TB efficacy models were employed.

312 Overall, our antimicrobial data are in accordance with the granuloma spectrum of
313 both mouse models discussed above where a more robust reduction in lung bacterial
314 burden was observed in the absence (Balb/c) versus the presence (C3HeB/FeJ) of

315 necrotic lesions. Both multidrug regimens as BPaL or BPaS significantly reduced lung
316 bacterial burden by 3.8-4.0 $\log_{10}$ and 2.5-2.7 $\log_{10}$ in Balb/c and C3HeB/FeJ TB models,
317 respectively (Figures 1E-H). We therefore conclude that both regimens promote similar
318 bactericidal effects in murine models lacking, or featuring, advanced pulmonary
319 pathology. Furthermore, the potent antimicrobial effect of the BPaL and BPaS regimens
320 also resulted in improvement of the pathological outcome during chronic infection with
321 Mtb but only the L-containing BPaL regimen, not BPaS, was associated with a
322 significant decrease in the live body weight at week 4 in Mtb-infected Balb/c and
323 C3HeB/FeJ mice (Figure 2C&D). The extent of weight loss is an important preclinical
324 and clinical parameter in TB patients because it determines the severity of disease
325 progression (38), and it is also an indicator of *in vivo* drug efficacy (39). The bactericidal
326 effects of S (as monotherapy) (40) and BPaL (41) in mice observed in these studies is
327 in line with previous reports and similar inverse relationship between body weight and L
328 exposure was recently reported in human patients (42).

329 Among L-associated hematological side effects, the incidence of anemia is
330 reported up to 62.5% in MDR and XDR-TB patients (43–45) and the onset of this effect
331 can occur 2 weeks to 2 months post L administration (46). In human TB patients treated
332 with anti-TB drugs (47–49), increased RDWs and lower HGB are associated with anemia
333 and these parameters serve as markers of disease prognosis. Using a CBC profile of 20
334 peripheral blood parameters, our preclinical study failed to detect any difference between
335 L or S 4-weeks monotherapy in terms of total red blood cells, white blood cells, platelets,
336 or hemoglobin (HGB) concentration compared to UnRx control (data not shown).
337 However, L treatment alone increased the RDWs and both L and S decreased the MCHC

338 (Figure 3A). Likewise, none of the 20-blood parameters evaluated showed any change
339 after the first 2 weeks of therapy with BPa, BPaL, or BPaS (Figure 3B). However, by 4
340 weeks, a significant drop in HGB and an increase in the RDWs was apparent for the BPaL
341 group (Figure 3B). This is interpreted to mean that mild hematological effects observed
342 in mice treated for 4 weeks with L or BPaL are dependent on the number of L-doses
343 administered and are thus, time-dependent. Overall, the onset of these hematological
344 effects when testing an L-containing regimen (BPaL) is in agreement with previous
345 studies (46,50) in human patients.

346 The mechanism of L-induced toxicity is attributed to its binding with the host
347 mitochondrial ribosomes leading to mitochondrial toxicities (17). The latter results in
348 activation of Nlrp3 inflammasome (51) and subsequently results in L-mediated bone
349 marrow myelosuppression (52); a phenomenon consistent with the hematologic
350 anomalies seen in patients treated with L for extended time periods. Because
351 spectinamides do not bind to mitochondrial ribosomes there is reduced potential for
352 similar side effects (16,18). To conclusively test this hypothesis, we performed bone
353 marrow histopathology to quantify the myeloid to erythroid ratio (M:E), a parameter that
354 provides information about the relative proportions of myeloid lineage (granulocytes,
355 monocytes, and their precursors) to erythroid lineage (53). The BPa and BPaL regimens
356 altered M:E in the C3HeB/FeJ TB model by suppressing myeloid and inducing erythroid
357 lineages (Figure 3C&D) whereas no such difference was observed in mice treated with
358 BPaS compared to untreated control. L was previously shown to impact M:E ratio,
359 although an opposite trend was observed in those studies, which employed 12-days of

360 L administration and a different strain of otherwise healthy mice (51). Time course
361 studies using a single consistent assay method are needed to resolve this discrepancy.
362 Elevation of interleukin 1β (IL-1β) levels and activation of Nlrp3 inflammasome
363 have been previously linked to myelosuppression (52). A 26-plexed immunoassay on
364 bone marrow samples from Mtb-infected C3HeB/FeJ mice revealed that most of the
365 proinflammatory cytokines and chemokines including IL-1β, IL-12p70 and TNF-α were
366 present at significantly higher concentrations in animals treated with BPaL compared to
367 BPaS (Figure 4A&B). The presence of elevated IL-1β was previously reported during
368 monotherapy with L (51,54). Studies from UnRx Mtb-infected C3HeB/FeJ mice also
369 revealed highly elevated levels of cytokines and chemokines (Figure 4C). As expected,
370 the positive therapeutic effect of BPaL and BPaS (as seen by reduction in bacterial and
371 lesion burden of lungs) also correlated with decreased level of proinflammatory
372 cytokines in bone marrow, lung, and plasma (Figures 4C, S12 and S13 respectively).
373 Similar to changes observed for cytokine profile, the flow cytometry data of bone
374 marrow, blood, and lungs along with quantification of mfIHC lung image analysis
375 revealed a significant change in the percentage of myeloid and lymphoid phenotypes
376 during treatment compared to UnRx control (Figures 5 and 6). Most notably, the
377 therapeutic effect of the BPa, BPaL and BPaS treatments reduced inflammatory
378 myeloid cells expressing CCR2 in blood and bone marrow and reduction in cytotoxic T
379 cells (CD3+CD8+) and γδT cells (CD3+CD8+γδTCR+) in lungs. In addition, BPa, BPaL
380 and BPaS therapy significantly increased the influx of helper T cells (CD3+CD4+),
381 regulatory T cells (Foxp3+) and B cells (CD3-CD19+) in lungs. These results suggest

382 that the combination therapy promotes the immune system's equilibrium by reducing
383 inflammation and enhancing adaptive immune responses.
384 An additional striking finding from this study was a strong concordance between
385 the decrease in lung and spleen bacterial burden and a corresponding decrease in the
386 number of cells expressing the neutrophil associated marker (Ly6G) (Figure 6C&D). An
387 implication of this finding is that the favorable treatment outcomes may promote a
388 corresponding decline in Ly6G neutrophil population as suggested before (55). Among
389 all immune cell phenotypes studied, no differences were found between BPaL and
390 BPaS treated animals and only the F4/80 +cells in the BPaS (but not in the BPaL)
391 treated animals showed significant increase when compared to the UnRx control.
392 The TB drug development field is working towards developing shorter and safer
393 therapies with a common goal of developing new multidrug regimens of low pill burden
394 that are accessible to patients, of short duration (ideally 2-3 months) and consist of 3-4
395 drugs of novel mode-of-action with proven efficacy, safety, and limited toxicity. Here we
396 present initial results that are in line with these goals. Further studies with inhaled
397 spectinamide 1599 and BPa are therefore warranted to determine if 2-3 months of
398 treatment with BPaS, further reduces the bacterial burden and leads to sterilizing
399 activity without associated AEs.
400
401
402
403
404

405 **Materials and Methods**

406 Female C3HeB/FeJ and Balb/c mice at 6-8 weeks of age were purchased from
407 the Jackson Laboratories. All protocols and use of these animals were approved by the
408 Institutional Animal Care and Use Committee (IACUC) at CSU. Animals were infected
409 with a low dose aerosol infection of Mtb (Erdman strain; ATCC 35801) using an
410 inhalation exposure system (Glas-Col, Terre Haute, IN) calibrated to deliver ~50-100
411 colony forming units (CFU) to the lungs (22). Clinical observations (e.g., inactivity, rough
412 fur, hunched posture, increased respiratory rate or effort) were monitored daily and their
413 live body weights were taken weekly.

414 **Drug preparation and treatment**

415 Bedaquiline fumarate (B) and linezolid (L) were obtained from LKT laboratories,
416 pretomanid (Pa) from ChemShuttle and 1599 (S: dihydrochloride) was provided by Dr.
417 Lee at St. Jude Children's Research Hospital. B was administered at 25 mg/kg. Pa and
418 L were administered at 100 mg/kg each and S was delivered by inhalation in liquid form
419 at 50 and 100 mg/kg to Balb/c and C3HeB/FeJ mice, respectively. The drugs were
420 formulated in weekly batches according to the live body weight of the animals, aliquoted
421 for single daily dosing, and stored at 4 °C in the dark.

422 The drugs were prepared as reported previously (21). Drug treatment was
423 started 4 weeks post-aerosol infection for Balb/c and at 8-9 weeks post-aerosol infection
424 for C3HeB/FeJ mice to allow time for lung pathology to fully develop. All drugs were
425 administered once daily for 5 days/week for 4 weeks by oral (gavage) administration
426 except S which was administered 3 days/week by intrapulmonary aerosol delivery using

427 the Penn Century microsprayer as reported previously (22). B was administered in the
428 morning, Pa one hour after B and, L and S at least 4 hours after Pa.

429 **Necropsy**

430 After 4-weeks of treatment, C3HeB/FeJ and Balb/c mice were humanely
431 euthanized by CO_2 narcosis. Blood, lungs, spleen, femur and tibia bones were collected
432 from each mouse for further processing and analysis.

433 **Assessment of Efficacy**

434 The efficacy of the treatment was assessed by determining changes in bacterial
435 burden [measured as colony forming units (CFU)] in the lungs and spleen of animals at
436 necropsy. The lungs and spleen were homogenized and prepared as reported
437 previously (22). The lung homogenates were plated onto 7H11 agar plates
438 supplemented with 0.4% activated charcoal to reduce the carryover effect of drugs and
439 incubated at 37 ^{o}C for 6-8 weeks before the final CFU count. The remaining lung
440 homogenate was centrifuged, and the supernatant was collected and stored at -80 °C
441 for evaluation of cytokines and chemokines.

442 **Histopathology and lesion scoring**

443 The lungs were fixed in 4% paraformaldehyde (PFA) for 48 hours then
444 embedded in paraffin for histopathology. Sections from formalin fixed and paraffin
445 embedded (FFPE) tissues were cut at 5 µm, stained with hematoxylin and eosin (H&E)
446 and scanned at 40X magnification using multispectral automated PhenoImager (Akoya
447 Biosciences) for histopathological evaluation. The extent of lung lesion burden was
448 quantified in blinded digital images using an open-source QuPath software for image
449 analysis as described previously (56).

450 The sternum and one femur were fixed in 4% PFA and processed for histology.
451 To evaluate the myelosuppressive effect of the drugs, bone sections were cut at 5 μm
452 and stained with H&E. The number of myeloid and erythroid cells from 5 different
453 regions of the bone were blinded and then counted by a veterinary clinical pathologist.

454 **Bone marrow collection**

455 Briefly, a 0.6 mL sterile Eppendorf tube punctured at the bottom with the help of a
456 26-gauge needle was inserted into a 1.5 mL sterile Eppendorf tube. One end of the
457 epiphysis of the long bones was cut open to expose the bone marrow and placed down
458 into the small Eppendorf tube-system. The tubes were centrifuged at 10,000 x g for 15
459 seconds and the marrow was collected from the base of the large Eppendorf tube. The
460 bone marrow was resuspended in PBS and centrifuged again. Thereafter, the
461 supernatant was collected and stored at -80 °C for evaluation of cytokines and
462 chemokines while the bone marrow cells were saved in 4% PFA and freezing media for
463 further use in clinical pathology analysis and flow cytometry, respectively.

464 **Processing of blood**

465 For complete blood count (CBC) analysis of C3HeB/FeJ animals during the
466 treatment, blood was collected in K2-EDTA tubes via submandibular vein puncture as
467 described previously (57). The blood was immediately analyzed in VETSCAN® HM5
468 hematology analyzer (Zoetis).

469 At the time of necropsy, whole blood was collected via cardiac puncture in K2-
470 EDTA containing tubes. After adding an equal volume of PBS, the samples were
471 centrifuged at 800 × g for 10 min at 25 °C with the brake off (deceleration = 0). The top
472 plasma layer was collected and stored at -80 °C for evaluation of their cytokine's

473 content. The buffy coat was collected, washed and the erythrocytes were lysed using
474 Miltenyi RBC lysis buffer (Miltenyi, CA). The cells were washed and resuspended in 500
475 µL of complete DMEM media and prepared for flow cytometry analysis.

476 **Cytokine quantification**

477 Multiplex immunoassay was performed using a Luminex bead-based multiplex
478 ELISA kit (ProcartaPlex Mouse Cytokine & Chemokine Panel 1 26plex, reference #
479 EPXR260-26088-901, Invitrogen). Each sample was normalized to the total protein
480 concentration determined by Bicinchoninic acid (BCA) assay (Thermo Fisher). The BCA
481 and Luminex assay were performed according to the manufacturer's instructions and
482 the final stained samples were fixed with 4% PFA prior to acquisition. Sample data were
483 acquired on a MAGPIX instrument running xPONENT 4.3 software (Luminex Corp.).
484 Heatmaps were generated using R pheatmap package. Correlation analysis of cytokine
485 contents in bone marrow, plasma and lungs with the lung bacterial burden was
486 performed using the corrplot package in R.

487

488 **Immune cell populations analysis**

489 Single cell suspension of bone marrow, blood, and lungs from C3HeB/FeJ mice
490 was prepared as described previously (56). Cells counting, viability staining and cell
491 staining (Table S1) was performed accordingly (56). Samples were acquired using
492 Cytek Aurora™ 4-Laser spectral flow cytometer where 100,000 events were recorded.
493 Data were analyzed in FlowJo software (BD Biosciences) using manual gating (58).

494

495

496 **Multiplex fluorescent immunohistochemistry**

497 Five µm sections of FFPE lung tissues were stained for multiplex fluorescent
498 immunohistochemistry (mfIHC) by the Imaging Core at the University of Colorado,
499 Anschutz Medical Campus, Denver. The mfIHC was performed for a panel of 6-color
500 antibodies + DAPI using Opal-plex Tyramide Signal Amplification (TSA) technique using
501 a Leica Bond III autostainer. The details of antibodies and Opal fluorophores used are
502 given in Table S2. Each antibody was optimized using Opal 3-Plex Anti-Rb Detection Kit
503 (Akoya Biosciences Inc. cat# NEL830001KT) and stained with automated LabSat™
504 Research (Lunaphore Technologies SA, Epredia). Slides were scanned using
505 multispectral automated PhenoImager™ (Akoya Biosciences) and analyzed for several
506 immune cell populations using the inForm® tissue Finder (Version 2.4.8) and
507 Phenochart™ (Version 1.0.12) software (Akoya Biosciences).

508

509 **Statistical analysis.** Bacterial burden data were expressed as CFU which were Log_{10}-
510 transformed and analyzed using GraphPad Prism version 9.5.1 (GraphPad software, La
511 Jolla, CA). The statistical analysis was performed using a Tukey's multiple comparison
512 test as part of either one-way or two-way ANOVA and mixed-model effect where
513 necessary. The correlation analysis was performed using the spearman's correlation
514 test. Flow cytometry and mfIHC data were graphed in R studio and statistical evaluation
515 was performed using stats package in R.

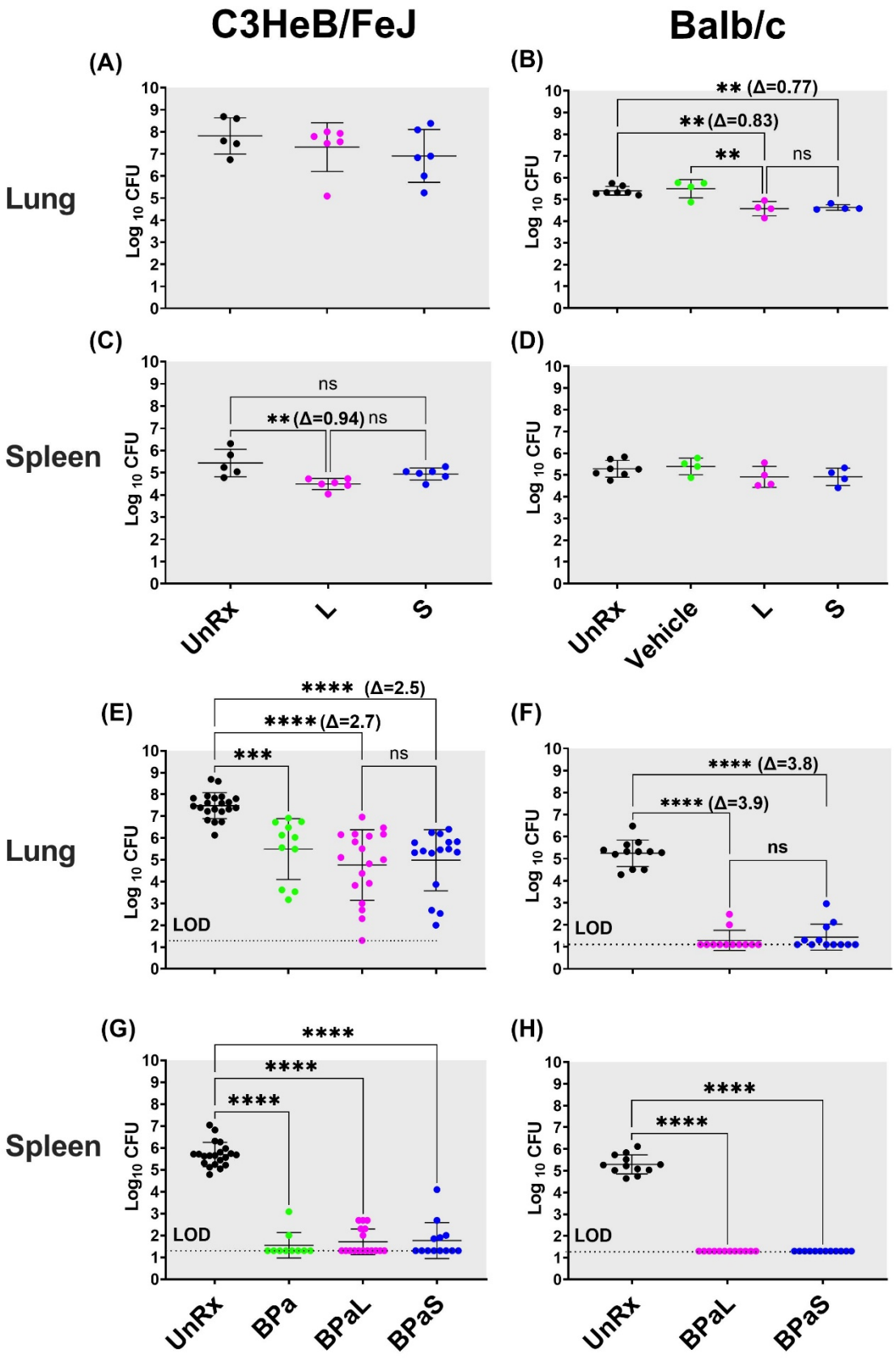
C3HeB/FeJ
Balb/c
(A)
(B)
Lung
Log 10 CFU
** (Δ=0.77)
** (Δ=0.83)
**
ns
(C)
(D)
Spleen
ns
** (Δ=0.94) ns
UnRx
L
S
Vehicle
(E)
(F)
**** (Δ=2.5)
**** (Δ=2.7)
***
ns
**** (Δ=3.8)
**** (Δ=3.9)
LOD
(G)
(H)
Log10 CFU
****
BPa
BPaL
BPaS

516

517 **Figure 1. Bactericidal effect of BPaL and BPaS in TB mouse models after 4-weeks**
518 **of treatment**

519 Balb/c and C3HeB/FeJ female mice were chronically infected with a low dose aerosol
520 infection of Mtb Erdman strain to deliver ~75 and ~100 bacilli respectively. Post-infection,
521 Balb/c and C3HeB/FeJ mice were rested for 4 and 8-9 weeks respectively until they were
522 randomly assigned to the study groups. The mice were treated with monotherapy of
523 linezolid or spectinamide 1599 or combination therapy of BPaL, BPa or BPaS for 4 weeks.
524 Bedaquiline (B), pretomanid (Pa) and linezolid (L) were administered at 25, 100 and 100
525 mg/kg respectively by oral gavage for 5/7 a week while spectinamide 1599 at 50 and 100
526 mg/kg in Balb/c and C3HeB/FeJ TB models respectively for 3/7 a week on the alternate
527 days via intrapulmonary aerosol delivery. On the third day of the last treatment, the mice
528 were euthanized, and their lungs and spleen were collected. The organs were
529 homogenized, serially diluted and plated on 7H11 agar with 4% charcoal (to avoid drug
530 carry-over effect) to determine bacterial burden in the form of colony forming units (CFU)
531 in each sample. CFU were enumerated after 4-6 weeks of incubation at 37 °C and
532 expressed as $\log_{10}$.C3HeB/FeJ and Balb/c TB models showing efficacy of monotherapy
533 (A-D) and combination therapy (E-H). The C3HeB/FeJ graphs (E&G) represent the
534 pooled data from three independent studies (n=3-8 each, Figures S1-3) and two of the
535 three studies contained BPa as a reference control. The Balb/c graphs (F&H) represent
536 the pooled data from two independent studies (n=5 each, Figures S7-8).
537 Statistical significance was calculated using one-way ANOVA with Tukey's multiple
538 comparison test, $p < 0.05$ was considered significant and ** = $p<0.001$, *** = $p<0.0001$,

539 **** = P<0.0001. UnRx = untreated, L = linezolid, S = spectinamide 1599, LOD: limit of

540 detection.

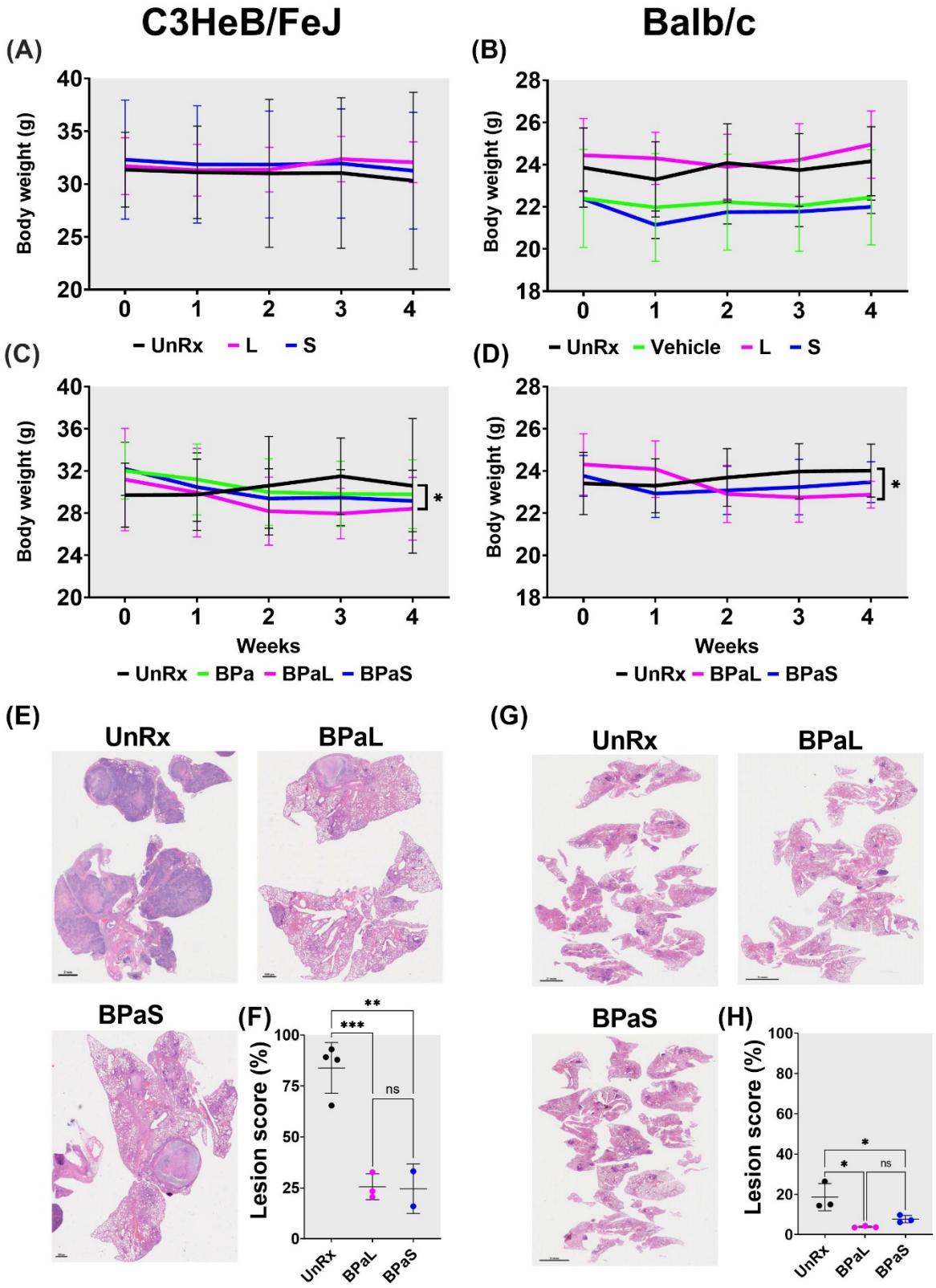
C3HeB/FeJ
Balb/c
(A)
(B)
(C)
(D)
Body weight (g)
Weeks
UnRx
L
S
Vehicle
BPa
BPaL
BPaS
*
(E)
(F)
(G)
(H)
UnRx
BPaL
BPaS
Lesion score (%)
**
***
ns

541

542 **Figure 2. Effect of therapy on the live body weight and lung histopathology of TB**
543 **mouse models after 4-weeks of treatment**

544 The live body weight of animals in Figure 1 treated with monotherapy (A&B) or multidrug
545 therapy (C&D) was recorded on a weekly basis. The average weight and SEM of each
546 group is shown. At the end of therapy, the mice were euthanized, and their lungs were
547 collected and processed for histopathology and lesion scoring (E-H). FFPE sections were
548 cut at 5 μm, stained with hematoxylin and eosin (H&E) and imaged at 40x (E&G). Lesion
549 scores (F&H) were calculated as the proportion of infected area over the total lung area
550 per animal. Statistical significance was calculated using mixed-effect model (body weight)
551 and one-way ANOVA (lesion score) with Tukey's multiple comparison test, and $p < 0.05$
552 was considered significant and ** = $p<0.001$, *** = $P<0.0001$. UnRx = untreated, L =

553 linezolid, S = spectinamide 1599

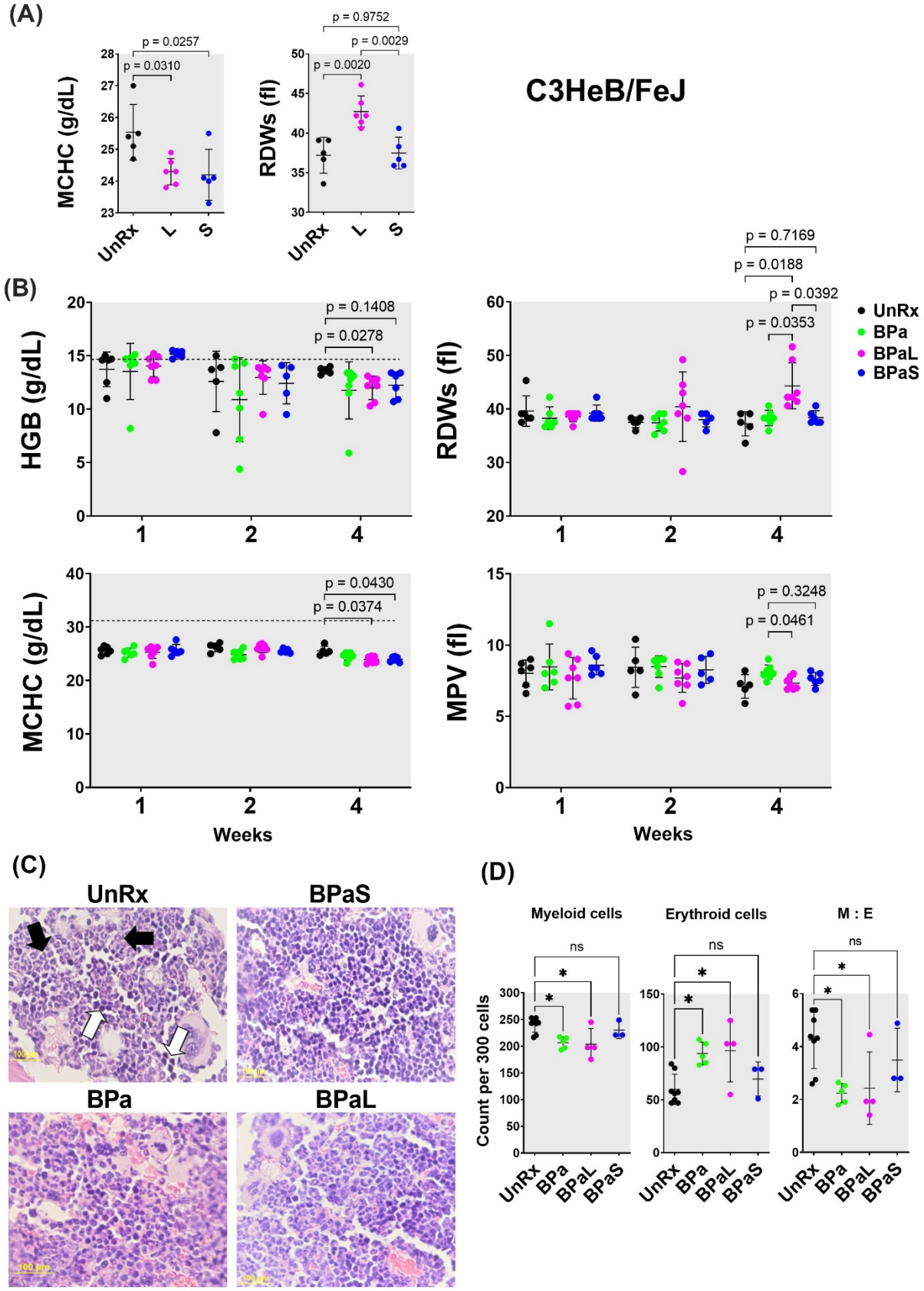
(A)
C3HeB/FeJ
MCHC (g/dL)
p = 0.0257
p = 0.0310
UnRx
L
S
RDWs (fl)
p = 0.9752
p = 0.0029
p = 0.0020
(B)
HGB (g/dL)
p = 0.1408
p = 0.0278
RDWs (fl)
p = 0.7169
p = 0.0188
p = 0.0392
p = 0.0353
UnRx
BPa
BPaL
BPaS
MCHC (g/dL)
p = 0.0430
p = 0.0374
MPV (fl)
p = 0.3248
p = 0.0461
Weeks
(C)
UnRx
BPaS
BPa
BPaL
(D)
Myeloid cells
Erythroid cells
M : E
Count per 300 cells
ns
*

554

555 **Figure 3. Complete blood count profiling and bone marrow histopathology of Mtb**
556 **infected C3HeB/FeJ TB model during 4-weeks of therapy**
557
558 During therapy of mice in Figure 1, the blood of live animals was collected at 1- and 2-
559 weeks via the puncture of submandibular vein. At the end of 4-weeks therapy, the blood
560 was collected by cardiac puncture. Blood was collected in K2-EDTA (purple top) tube and
561 immediately analyzed for the complete blood count in VETSCAN® HM5 hematology
562 analyzer (Zoetis). (A) monotherapy, (B) multidrug therapy. The MCHC (mean corpuscular
563 hemoglobin concentration) and RDWs (red blood cell distribution width-standard
564 deviation) along with the HGB (hemoglobin concentration) and MPV (mean platelet
565 volume) are shown. A horizontal dotted line indicates the lower end of the reference
566 interval for C3HeB/FeJ mice.
567
568 The sternum, femur and tibias bones from each mouse were collected, fixed in 4% PFA,
569 and processed for histology (C&D). Sections were cut at 5 μm, stained with hematoxylin
570 and eosin (H&E) and imaged at 40x. (C) Representative photos of bone marrow sections
571 showing myeloid (black arrows) and erythroid (white arrows) cells in bone marrow of
572 untreated (UnRx) and treatment (BPa, BPaS and BPaS) groups. (D) The number of
573 myeloid (M) and erythroid (E) among a total of 300 cells in 5 different regions were
574 counted for each group and M:E was calculated. Statistical significance was calculated
575 using one-way ANOVA with Tukey's test for multiple comparisons. $p < 0.05$ was
576 considered significant and ** = $p<0.001$, *** = $P<0.0001$.
577
578

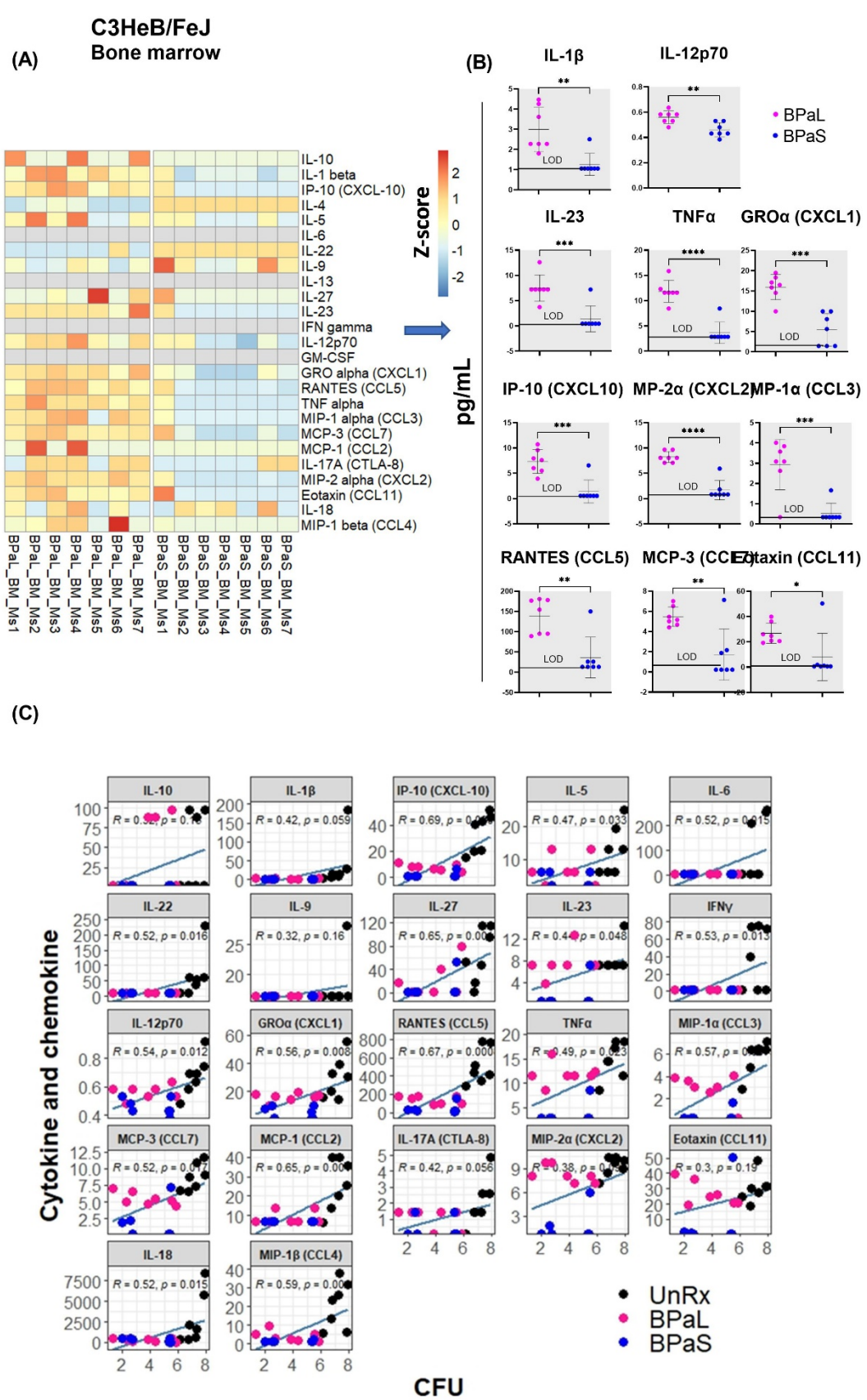
C3HeB/FeJ
Bone marrow
(A)
(B)
(C)
IL-10
IL-1 beta
IP-10 (CXCL-10)
IL-4
IL-5
IL-6
IL-22
IL-9
IL-13
IL-27
IL-23
IFN gamma
IL-12p70
GM-CSF
GRO alpha (CXCL1)
RANTES (CCL5)
TNF alpha
MIP-1 alpha (CCL3)
MCP-3 (CCL7)
MCP-1 (CCL2)
IL-17A (CTLA-8)
MIP-2 alpha (CXCL2)
Eotaxin (CCL11)
IL-18
MIP-1 beta (CCL4)
Z-score
BPaL_BM_Ms1
BPaL_BM_Ms2
BPaL_BM_Ms3
BPaL_BM_Ms4
BPaL_BM_Ms5
BPaL_BM_Ms6
BPaL_BM_Ms7
BPaS_BM_Ms1
BPaS_BM_Ms2
BPaS_BM_Ms3
BPaS_BM_Ms4
BPaS_BM_Ms5
BPaS_BM_Ms6
BPaS_BM_Ms7
pg/mL
BPaL
BPaS
LOD
IL-1β
IL-12p70
IL-23
TNFα
GROα (CXCL1)
IP-10 (CXCL10)
MP-2α (CXCL2)
MP-1α (CCL3)
RANTES (CCL5)
MCP-3 (CCL7)
Eotaxin (CCL11)
Cytokine and chemokine
CFU
UnRx
BPaL
BPaS

620 **Figure 4. Bone marrow cytokine and chemokine profiling in Mtb infected**

621 **C3HeB/FeJ TB model after 4-weeks of treatment**

622 Femur bones from selected studies in mice in Figure 1 were collected to harvest the bone
623 marrow. The bone marrow was resuspended in PBS, centrifuged and the supernatant
624 was collected for the evaluation of cytokine's content. BPaL and BPaS therapy showed
625 profile of 26 cytokines and chemokines in bone marrow and the data were converted to
626 Z score and represented as a heatmap (A) and graphically (B). (C) Spearman's
627 correlation analysis of bone marrow cytokines and chemokines with the lung bacterial
628 burden (CFU).

629 Statistical significance was calculated using the t test. $p < 0.05$ was considered significant
630 and ** = $p<0.001$*** = $p<0.0001$, **** = $P<0.00001$.

631

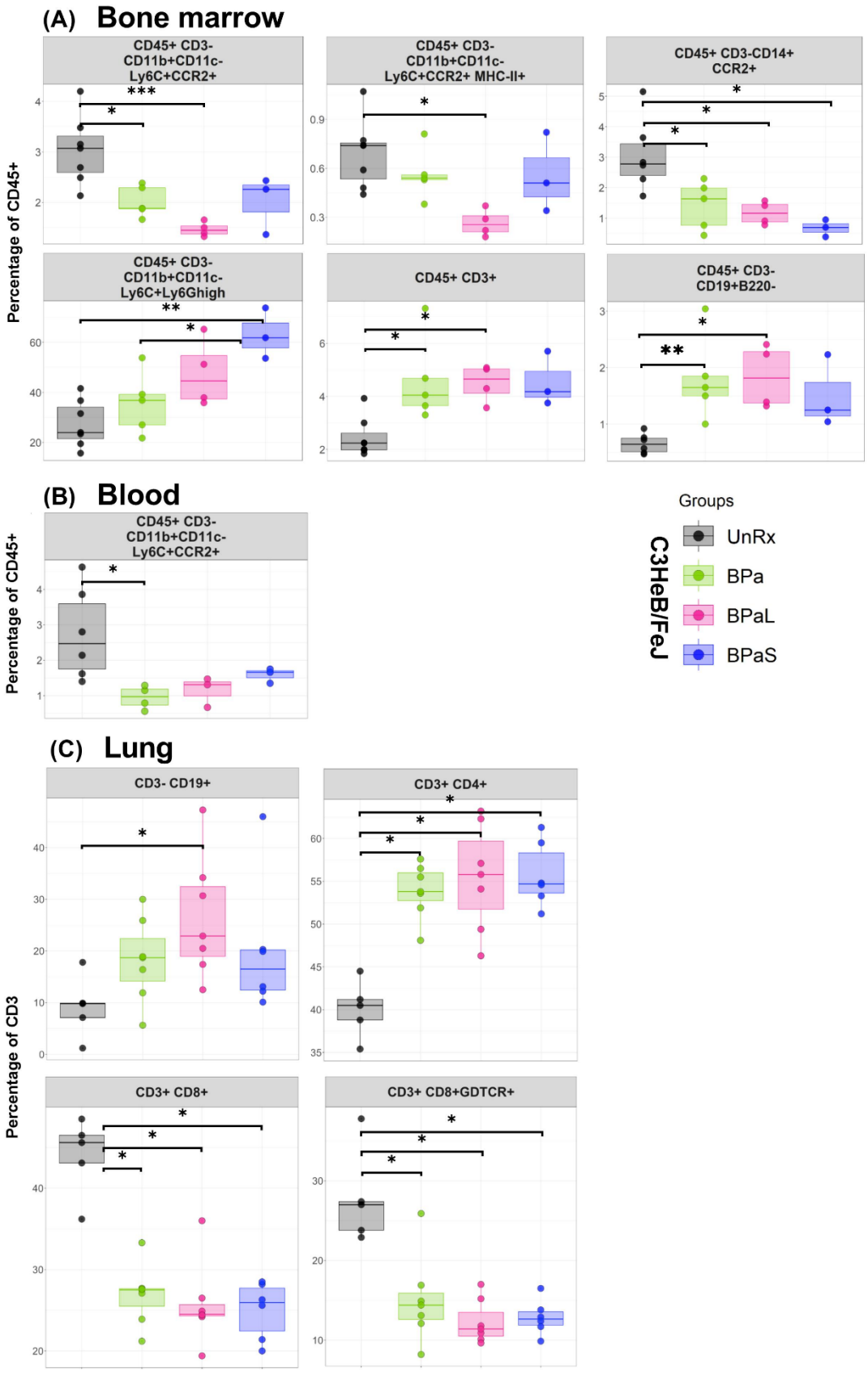
(A) Bone marrow
CD45+ CD3- CD11b+CD11c- Ly6C+CCR2+
CD45+ CD3- CD11b+CD11c- Ly6C+CCR2+ MHC-II+
CD45+ CD3-CD14+ CCR2+
CD45+ CD3- CD11b+CD11c- Ly6C+Ly6Ghigh
CD45+ CD3+
CD45+ CD3- CD19+B220-
Percentage of CD45+
(B) Blood
CD45+ CD3- CD11b+CD11c- Ly6C+CCR2+
Percentage of CD45+
Groups
UnRx
BPa
BPaL
BPaS
C3HeB/FeJ
(C) Lung
CD3- CD19+
CD3+ CD4+
CD3+ CD8+
CD3+ CD8+GDTCR+
Percentage of CD3

660 **Figure 5. Immune cell populations in the bone marrow, lung and blood of**
661 **C3HeB/FeJ TB model after 4-weeks of treatment**

662 The bone marrow, lung and blood from selected studies from Figure 1 were evaluated by
663 flow cytometry. The samples were processed for a panel of 17-color antibodies and the
664 data were analyzed by FlowJo software using manual gating strategy. The myeloid and
665 lymphoid phenotypes present in the untreated (UnRx) and treatment (BPa, BPaL or
666 BPaS) groups are shown. Statistical significance was calculated using one-way ANOVA
667 with Tukey's test for multiple comparisons. $p < 0.05$ was considered significant and ** =
668 $p<0.001$*** = $p<0.0001$, **** = $P<0.00001$.

669

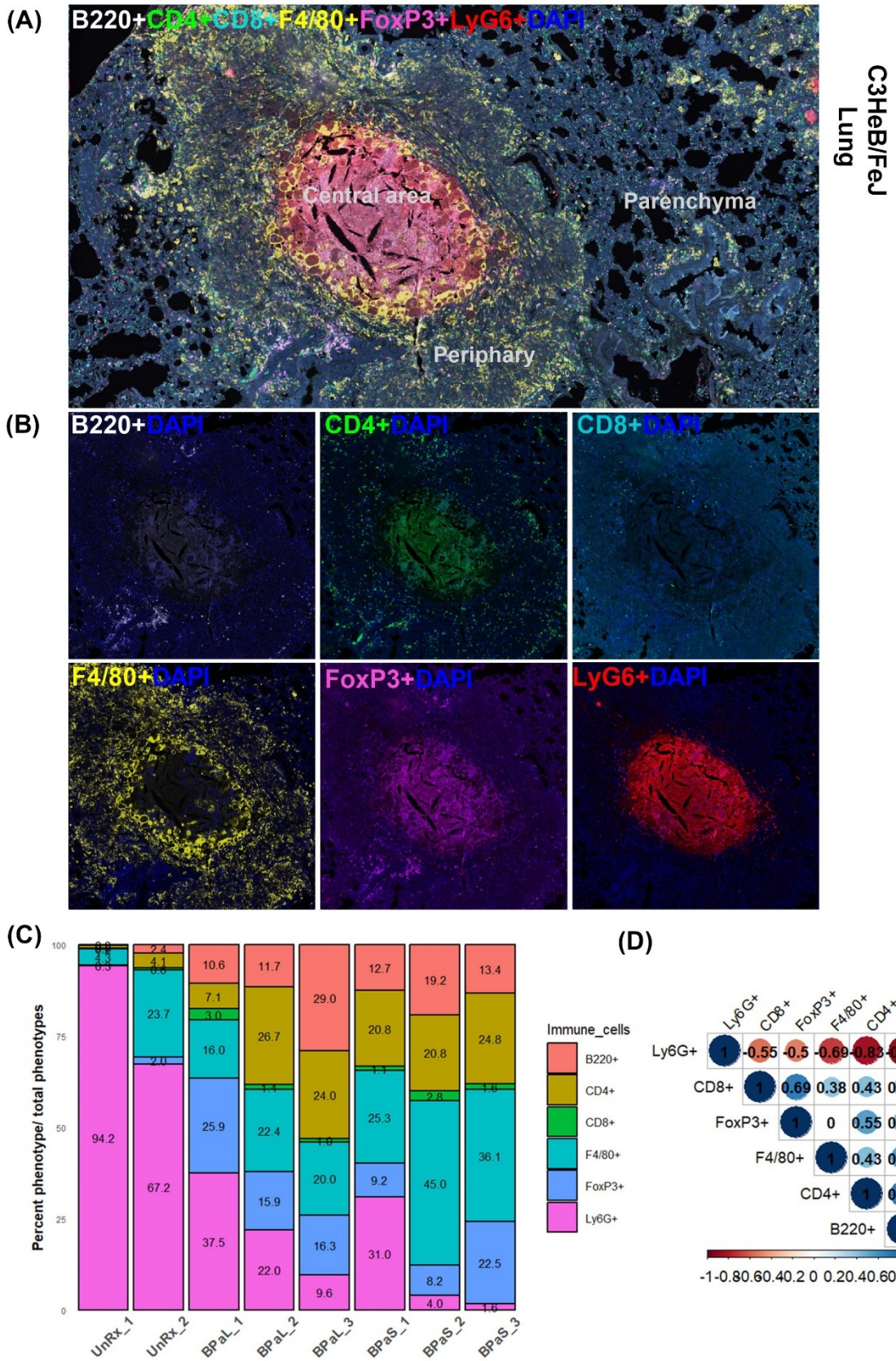
(A)
B220+CD4+CD8+F4/80+FoxP3+LyG6+DAPI
Central area
Parenchyma
Periphary
C3HeB/FeJ
Lung
(B)
B220+DAPI
CD4+DAPI
CD8+DAPI
F4/80+DAPI
FoxP3+DAPI
LyG6+DAPI
(C)
Percent phenotype/ total phenotypes
UnRx_1
UnRx_2
BPaL_1
BPaL_2
BPaL_3
BPaS_1
BPaS_2
BPaS_3
Immune_cells
B220+
CD4+
CD8+
F4/80+
FoxP3+
Ly6G+
(D)
Ly6G+
CD8+
FoxP3+
F4/80+
CD4+
B220+
-1 -0.8 -0.6 -0.4 -0.2 0 0.2 0.4 0.6 0.8 1

670

671 **Figure 6. Immune cell populations in the lungs of Mtb infected C3HeB/FeJ TB**
672 **model after 4-weeks of treatment**
673
674 Selected mice from those shown in Figure 1 were processed for multiplex fluorescent
675 immunohistochemistry (mfIHC). The mfIHC was performed for a panel of 6-color
676 antibodies + DAPI using Opal-plex Tyramide Signal Amplification (TSA). Slides were
677 scanned using multispectral automated PhenoImager™ (Akoya Biosciences) and
678 analyzed for different immune cell populations using the inForm® tissue Finder and
679 Phenochart software (Akoya Biosciences). (A) The lung mfIHC full composite image
680 displays B220, CD4, CD8, F4/80, FoxP3 and Ly6G markers along with DAPI staining for
681 nuclei in the TB granuloma. The central and peripheral regions of a TB granuloma and
682 the parenchyma of lung are also shown. (B) Single color composite image of individual
683 markers with DAPI showing distribution of each immune cell population in the TB
684 granuloma. (C) Cell populations (%) of several immune cells per total number of
685 phenotypes calculated in untreated (UnRx) and treatment (BPaL and BPaS) groups
686 based on a panel of 6-color antibodies + DAPI. (D) Spearman's correlation matrix for
687 several immune cell populations (B220, CD4, CD8, F4/80, FoxP3, Ly6G) showing all
688 relationships. A coefficient with a value of either +1 (blue), 0 (white), or -1 (red) indicates
689 a perfect association, no association, and a perfect negative association of ranks,
690 respectively. Numbers indicate the correlation coefficient.

Acknowledgments: This research was supported by the National Institute of Allergy and Infectious Diseases and the Office of the Director of the National Institutes of Health (grants R01AI120670, R01AI090810 and 1S10OD030263 respectively). Dr. Malik Zohaib Ali was a Fulbright Foreign Student Program grantee from Pakistan. Dr. Charles Daley from the Division of Mycobacterial and Respiratory Infections, National Jewish Health, Denver, Colorado 80206, USA advised on current TB drug treatments. The content is solely the responsibility of the authors and does not necessarily represent the official views of the National Institutes of Health. We acknowledge the staff of the Laboratory Animal Resources at Colorado State University for providing animal care.

700 **References**

701 1. Campbell JR, Nsengiyumva P, Chiang LY, Jamieson F, Khadawardi H, Mah HKH,
702 et al. Costs of Tuberculosis at 3 Treatment Centers, Canada, 2010–2016. Emerg
703 Infect Dis. 2022;28(9):1814–23.

704 2. Zhang MW, Zhou L, Zhang Y, Chen B, Peng Y, Wang F, et al. Treatment
705 outcomes of patients with multidrug and extensively drug-resistant tuberculosis in
706 Zhejiang, China. Eur J Med Res. 2021;26(1):1–10.

707 3. Williams K, Minkowski A, Amoabeng O, Peloquin CA, Taylor D, Andries K, et al.
708 Sterilizing activities of novel combinations lacking first- and second-line drugs in a
709 murine model of tuberculosis. Antimicrob Agents Chemother. 2012;56(6):3114–
710 20.

711 4. Tasneen R, Betoudji F, Tyagi S, Li SY, Williams K, Converse PJ, et al.
712 Contribution of oxazolidinones to the efficacy of novel regimens containing
713 bedaquiline and pretomanid in a mouse model of tuberculosis. Antimicrob Agents
714 Chemother. 2016;60(1):270–7.

715 5. Conradie F, Diacon AH, Ngubane N, Howell P, Everitt D, Crook AM, et al.
716 Treatment of Highly Drug-Resistant Pulmonary Tuberculosis. N Engl J Med.
717 2020;382(10):893–902.

718 6. Conradie F, Bagdasaryan TR, Borisov S, Howell P, Mikiashvili L, Ngubane N, et
719 al. Bedaquiline–Pretomanid–Linezolid Regimens for Drug-Resistant Tuberculosis.

720 N Engl J Med. 2022;387(9):810–23.

721 7. TB-Alliance. Update on Pretomanid , in Combination with Bedaquiline and
722 Linezolid (the BPaL Regimen) in Drug-Resistant TB. 2022.

723 8. Jackson A. Foresight. In: Drugs and the Future: Brain Science, Addiction and
724 Society. 2006. p. 7–10.

725 9. Richter E, Rüsch-Gerdes S, Hillemann D. First linezolid-resistant clinical isolates
726 of Mycobacterium tuberculosis. Antimicrob Agents Chemother. 2007;51(4):1534–
727 6.

728 10. Li SY, Converse PJ, Betoudji F, Lee J, Mdluli K, Upton A, et al. Next-Generation
729 Diarylquinolines Improve Sterilizing Activity of Regimens with Pretomanid and the
730 Novel Oxazolidinone TBI-223 in a Mouse Tuberculosis Model. Antimicrob Agents
731 Chemother. 2023;67(4):1–9.

732 11. Holloway WJ. Spectinomycin. Med Clin North Am. 1982;66(1).

733 12. Kanchugl, S. and Selmer M. Structural Recognition of Spectinomycin by
734 Resistance Enzyme ANT(9) from Enterococcus faecalis. Antimicrob Agents
735 Chemother. 2020;64(June):e00371-20.

736 13. Owusu E, Amartey BT, Afutu E, Boafo N. Aminoglycoside Therapy for
737 Tuberculosis: Evidence for Ototoxicity among Tuberculosis Patients in Ghana.
738 Diseases. 2022;10(1):10.

739 14. De Jager R, Van Altena R. Hearing loss and nephrotoxicity in long-term

740 aminoglycoside treatment in patients with tuberculosis. Int J Tuberc Lung Dis.
741 2002;6(7):622–7.

742 15. Temrikar ZH, Kodidela S, Kumar S, Liu J, Robertson GT, Lee RE, et al.
743 Characterization of spectinamide 1599 efficacy against different mycobacterial
744 phenotypes. Tuberculosis [Internet]. 2023;140(April):102342. Available from:
745 https://doi.org/10.1016/j.tube.2023.102342

746 16. Richard E. Lee, Julian G. Hurdle, Jiuyu Liu, David F. Bruhn, Tanja Matt, Michael
747 S. Scherman, Pavan K Vaddady, Zhong Zheng, Jianjun Qi, Rashid Akbergenov,
748 Sourav Das, Dora B. Madhura, Chetan Rathi, Ashit Trivedi, Cristina Villellas,#,
749 Robin. B. Lee, Rakes and AJL. Spectinamides: A New Class of Semisynthetic
750 Anti-Tuberculosis Agents that Overcome Native Drug Efflux. Nat Med.
751 2017;20(2):152–8.

752 17. De Vriese AS, Van Coster R, Smet J, Seneca S, Lovering A, Van Haute LL, et al.
753 Linezolid-induced inhibition of mitochondrial protein synthesis. Clin Infect Dis.
754 2006;42(8):1111–7.

755 18. Modongo C, Pasipanodya JG, Zetola NM, Williams SM, Sirugo G, Gumboc T.
756 Amikacin concentrations predictive of ototoxicity in multidrug-resistant
757 tuberculosis patients. Antimicrob Agents Chemother. 2015;59(10):6337–43.

758 19. Liu J, Bruhn DF, Lee RB, Zheng Z, Janusic T, Scherbakov D, et al. Structure-
759 activity relationships of spectinamide antituberculosis agents: A dissection of
760 ribosomal inhibition and native efflux avoidance contributions. ACS Infect Dis.

761 2017;3(1):72–88.

762 20. Bruhn DF, Scherman MS, Liu J, Scherbakov D, Meibohm B, Böttger EC, et al. In
763 vitro and in vivo evaluation of synergism between anti-tubercular spectinamides
764 and non-classical tuberculosis antibiotics. Sci Rep. 2015;5(May):1–10.

765 21. Robertson GT, Scherman MS, Bruhn DF, Liu J, Hastings C, McNeil MR, et al.
766 Spectinamides are effective partner agents for the treatment of tuberculosis in
767 multiple mouse infection models. J Antimicrob Chemother. 2017;72(3):770–7.

768 22. Gonzalez-Juarrero M, Lukka PB, Wagh S, Walz A, Arab J, Pearce C, et al.
769 Preclinical Evaluation of Inhalational Spectinamide-1599 Therapy against
770 Tuberculosis. ACS Infect Dis. 2021;7(10):2850–63.

771 23. Wagh S, Rathi C, Lukka PB, Parmar K, Temrikar Z, Liu J, et al. Model-based
772 exposure-response assessment for spectinamide 1810 in a mouse model of
773 tuberculosis. Antimicrob Agents Chemother. 2021;65(11):1–15.

774 24. Nirmal A, Sznajder K, Patil R, Shaikh B. Preference of inhalants over
775 pills/injections among pulmonary tuberculosis patients in Western India: A cross-
776 sectional study. J Clin Tuberc Other Mycobact Dis. 2021;23.

777 25. Matthieu B, Matthieu J, Nicolas G, Patrice G, Srine M, William C, et al.
778 Comparison of intrapulmonary and systemic pharmacokinetics of colistin
779 methanesulfonate (CMS) and colistin after aerosol delivery and intravenous
780 administration of CMS in critically ill patients. Antimicrob Agents Chemother.
781 2014;58(12):7331–9.

782 26. Rathi C, Lukka PB, Wagh S, Lee RE, Lenaerts AJ, Braunstein M, et al.
783 Comparative pharmacokinetics of spectinamide 1599 after subcutaneous and
784 intrapulmonary aerosol administration in mice. Tuberculosis. 2019;114(December
785 2018):119–22.

786 27. Hickey AJ, Misra A, Fourie PB. Dry powder antibiotic aerosol product
787 development: Inhaled therapy for tuberculosis. J Pharm Sci [Internet].
788 2013;102(11):3900–7. Available from: http://dx.doi.org/10.1002/jps.23705

789 28. Irwin SM, Driver E, Lyon E, Schrupp C, Ryan G, Gonzalez-Juarrero M, et al.
790 Presence of multiple lesion types with vastly different microenvironments in
791 C3HeB/FeJ mice following aerosol infection with Mycobacterium tuberculosis.
792 DMM Dis Model Mech. 2015;8(6):591–602.

793 29. Driver ER, Ryan GJ, Hoff DR, Irwin SM, Basaraba RJ, Kramnik I, et al. Evaluation
794 of a mouse model of necrotic granuloma formation using C3HeB/FeJ mice for
795 testing of drugs against Mycobacterium tuberculosis. Antimicrob Agents
796 Chemother. 2012;56(6):3181–95.

797 30. Harper J, Skerry C, Davis SL, Tasneen R, Weir M, Kramnik I, et al. Mouse model
798 of necrotic tuberculosis granulomas develops hypoxic lesions. J Infect Dis.
799 2012;205(4):595–602.

800 31. Irwin SM, Gruppo V, Brooks E, Gilliland J, Scherman M, Reichlen MJ, et al.
801 Limited activity of clofazimine as a single drug in a mouse model of tuberculosis
802 exhibiting caseous necrotic granulomas. Antimicrob Agents Chemother.

803 2014;58(7):4026–34.

804 32. S Aly, K Wagner, C Keller, S Malm, A Malzan, S Brandau, Bange E. Oxygen
805 status of lung granulomas in Mycobacterium tuberculosis-infected mice. J Pathol.
806 2006;210:298–305.

807 33. Singh AK, Gupta UD. Animal models of tuberculosis: Lesson learnt. Indian J Med
808 Res [Internet]. 2018;147:456–63. Available from:
809 http://www.ncbi.nlm.nih.gov/pubmed/23144490

810 34. De Groote MA, Gilliland JC, Wells CL, Brooks EJ, Woolhiser LK, Gruppo V, et al.
811 Comparative studies evaluating mouse models used for efficacy testing of
812 experimental drugs against Mycobacterium tuberculosis. Antimicrob Agents
813 Chemother. 2011;55(3):1237–47.

814 35. Dpre, Robertson GT, Ramey ME, Massoudi LM, Carter CL, Zimmerman M, et al.
815 Comparative Analysis of Pharmacodynamics in the C3HeB / FeJ. Antimicrob
816 Agents Chemother aac.asm.org. 2021;65 Issue(July):e00583-21.

817 36. Lanoix JP, Lenaerts AJ, Nuermberger EL. Heterogeneous disease progression
818 and treatment response in a C3HeB/FeJ mouse model of tuberculosis. DMM Dis
819 Model Mech. 2015;8(6):603–10.

820 37. Walter ND, Ernest JP, Dide-Agossou C, Bauman AA, Ramey ME, Rossmassler K,
821 et al. Lung microenvironments harbor Mycobacterium tuberculosis phenotypes
822 with distinct treatment responses . Antimicrob Agents Chemother. 2023;67(9):1–
823 15.

824 38. Van Crevel R, Karyadi E, Netea MG, Verhoef H, Nelwan RHH, West CE, et al.
825 Decreased plasma leptin concentrations in tuberculosis patients are associated
826 with wasting and inflammation. J Clin Endocrinol Metab. 2002;87(2):758–63.

827 39. Nikonenko B V., Samala R, Einck L, Nacy CA. Rapid, simple in vivo screen for
828 new drugs active against Mycobacterium tuberculosis. Antimicrob Agents
829 Chemother. 2004;48(12):4550–5.

830 40. Pstragowski, M. Zbrzezna, M. and Bujalska-Zadrozny M. Advances in
831 pharmacotherapy of Tuberculosis [Internet]. Vol. 74, Acta Poloniae - Drug
832 Research. 2017. p. 3–11. Available from:
833 https://www.embase.com/search/results?subaction=viewrecord&id=L604925228&
834 from=export

835 41. Nuermberger EL, Martínez-Martínez MS, Sanz O, Urones B, Esquivias J, Soni H,
836 et al. GSK2556286 Is a Novel Antitubercular Drug Candidate Effective In Vivo
837 with the Potential To Shorten Tuberculosis Treatment. Vol. 66, Antimicrobial
838 Agents and Chemotherapy. 2022.

839 42. Wasserman S, Denti P, Brust JCM, Abdelwahab M, Hlungulu S, Wiesner L, et al.
840 Linezolid pharmacokinetics in South African patients with drug-resistant
841 tuberculosis and a high prevalence of HIV coinfection. Antimicrob Agents
842 Chemother. 2019;63(3).

843 43. Abebe G, , Zegeye Bonsa WK. Early Safety and Efficacy of Linezolid-Based
844 Combination Therapy among Patients with Drug-Resistant Tuberculosis in

845 North-western Nigeria. Int J Mycobacteriology. 2021;10:129–35.

846 44. Palomino JC, Martin A. Drug resistance mechanisms in Mycobacterium
847 tuberculosis. Antibiotics. 2014;3(3):317–40.

848 45. Sotgiu G, Centis R, D'Ambrosio L, Alffenaar JWC, Anger HA, Caminero JA, et al.
849 Efficacy, safety and tolerability of linezolid containing regimens in treating MDR-
850 TB and XDR-TB: Systematic review and meta-analysis. Eur Respir J.
851 2012;40(6):1430–42.

852 46. Tang S, Yao L, Hao X, Zhang X, Liu G, Liu X, et al. Efficacy, safety and tolerability
853 of linezolid for the treatment of XDR-TB: A study in China. Eur Respir J [Internet].
854 2015;45(1):161–70. Available from: http://dx.doi.org/10.1183/09031936.00035114

855 47. Nezamodini ZS, Rezvani Z, Kian K. Electronic Physician (ISSN : 2008-5842).
856 Electron Physician. 2017;9(January):3592–7.

857 48. Kassa E, Enawgaw B, Gelaw A, Gelaw B. Effect of anti-tuberculosis drugs on
858 hematological profiles of tuberculosis patients attending at University of Gondar
859 Hospital, Northwest Ethiopia. BMC Hematol. 2016;16(1):1–11.

860 49. Luo M, Liu M, Wu X, Wu Y, Yang H, Qin L, et al. Impact of anemia on prognosis
861 in tuberculosis patients. Ann Transl Med. 2022;10(6):329–329.

862 50. Gerson SL, Kaplan SL, Bruss JB, Le V, Arellano FM, Hafkin B, et al. Hematologic
863 effects of linezolid: Summary of clinical experience. Antimicrob Agents
864 Chemother. 2002;46(8):2723–6.

865 51. Iyer SS, Iyer SS, He Q, He Q, Janczy JR, Janczy JR, et al. Mitochondrial
866 Cardiolipin Is Required for Nlrp3 Inflammasome Activation. Immunity [Internet].
867 2013;39(2):311–23. Available from:
868 http://linkinghub.elsevier.com/retrieve/pii/S1074761313003294%5Cnpapers3://pu
869 blication/doi/10.1016/j.immuni.2013.08.001

870 52. Winchell CG, Mishra BB, Phuah JY, Saqib M, Nelson SJ, Maiello P, et al.
871 Evaluation of IL-1 Blockade as an Adjunct to Linezolid Therapy for Tuberculosis in
872 Mice and Macaques. Front Immunol. 2020;11(May):1–18.

873 53. Elmore SA. Enhanced Histopathology of the Bone Marrow Susan. Toxicol Pathol
874 [Internet]. 2006;34(5):666–86. Available from:
875 https://www.ncbi.nlm.nih.gov/pmc/articles/PMC3624763/pdf/nihms412728.pdf

876 54. Jasenosky LD, Scriba TJ, Hanekom WA, Goldfeld AE. T cells and adaptive
877 immunity to Mycobacterium tuberculosis in humans. Immunol Rev.
878 2015;264(1):74–87.

879 55. Lovewell RR, Baer C, Mishra BB, Smith CM, Christopher M. Granulocytes act as
880 a niche for Mycobacterium tuberculosis growth. Mucosal Immunol.
881 2021;14(1):229–41.

882 56. Dutt TS, Karger BR, Fox A, Youssef N, Dadhwal R, Ali MZ, et al. Mucosal
883 exposure to non-tuberculous mycobacteria elicits B cell-mediated immunity
884 against pulmonary tuberculosis. Cell Rep [Internet]. 2022;41(11):111783.
885 Available from: https://doi.org/10.1016/j.celrep.2022.111783

886 57. Golde WT, Gollobin P, Rodriguez LL. A rapid, simple, and humane method for
887 submandibular bleeding of mice using a lancet. Lab Anim (NY). 2005;34(9):39–
888 43.

889 58. Fox A, Dutt TS, Karger B, Rojas M, Obregón-Henao A, Anderson GB, et al. Cyto-
890 Feature Engineering: A Pipeline for Flow Cytometry Analysis to Uncover Immune
891 Populations and Associations with Disease. Sci Rep. 2020;10(1):1–12.

892

893

894 ## Supporting information

895 **Figure S1 (C3HeB/FeJ Study 1).** Bacterial burden (CFU) in Mtb infected C3HeB/FeJ mice treated with
896 BPaL and BPaS regimen for 4 weeks

897 **Figure S2 (C3HeB/FeJ Study 2).** Bacterial burden (CFU) in Mtb infected C3HeB/FeJ mice treated with
898 BPa, BPaL and BPaS regimen for 4 weeks

899 **Figure S3 (C3HeB/FeJ Study 3).** Bacterial burden (CFU) in Mtb infected C3HeB/FeJ mice treated with
900 BPa, BPaL and BPaS regimen for 4 weeks

901 **Figure S4 (C3HeB/FeJ Study 1).** Change in the average live body weight of Mtb infected C3HeB/FeJ mice
902 during drug treatment

903 **Figure S5 (C3HeB/FeJ Study 2).** Change in the average live body weight of Mtb infected C3HeB/FeJ mice
904 during drug treatment

905 **Figure S6 (C3HeB/FeJ Study 3).** Change in the average live body weight of Mtb infected C3HeB/FeJ mice
906 during drug treatment

907 **Figure S7 (Balb/c Study 1).** Bacterial burden (CFU) in Mtb infected Balb/c mice treated with BPaL and
908 BPaS regimen for 4 weeks

909 **Figure S8 (Balb/c Study 2).** Bacterial burden (CFU) in Mtb infected Balb/c mice treated with BPaL and
910 BPaS regimen for 4 weeks

911 **Figure S9 (Balb/c Study 1).** Change in the average live body weight of Mtb infected Balb/c mice during
912 drug treatment

913 **Figure S10 (Balb/c Study 2).** Change in the average live body weight of Mtb infected Balb/c mice during

914 drug treatment

915 **Figure S11**. Change in the cytokines and chemokines profile in Mtb infected C3HeB/FeJ mice during drug
916 treatment

917 **Figure S12**. Spearman's correlation analysis between bacterial burden (CFU) and cytokine and
918 chemokine profile in the lungs of Mtb infected C3HeB/FeJ mice treated with BPaL and BPaS regimen
919

920 **Figure S13**. Spearman's correlation analysis between lung bacterial burden (CFU) and plasma cytokine
921 and chemokine profile in Mtb infected C3HeB/FeJ mice treated with BPaL and BPaS regimen
922

923 **Figure S14.** Immune cell populations in the lungs of Mtb infected C3HeB/FeJ TB model after 4 weeks
924 therapy
925

926 **Table S1**. **Reagents**
927

928 **Table S2. Antibodies**